Robust Vector Quantized-Variational Autoencoder

Chieh-Hsin Lai [1] **Dongmian Zou** [2] **Gilad Lerman** [1]

Abstract

Image generative models can learn the distributions of the training data and consequently generate examples by sampling from these distributions. However, when the training dataset is corrupted with outliers, generative models will likely produce examples that are also similar to the outliers. In fact, a small portion of outliers may induce state-of-the-art generative models, such as Vector Quantized-Variational AutoEncoder (VQ-VAE), to learn a significant mode from the outliers. To mitigate this problem, we propose a robust generative model based on VQ-VAE, which we name Robust VQ-VAE (RVQ-VAE). In order to achieve robustness, RVQ-VAE uses two separate codebooks for the inliers and outliers. To ensure the codebooks embed the correct components, we iteratively update the sets of inliers and outliers during each training epoch. To ensure that the encoded data points are matched to the correct codebooks, we quantize using a weighted Euclidean distance, whose weights are determined by directional variances of the codebooks. Both codebooks, together with the encoder and decoder, are trained jointly according to the reconstruction loss and the quantization loss. We experimentally demonstrate that RVQ-VAE is able to generate examples from inliers even if a large portion of the training data points are corrupted.

1. Introduction

In the past several years, deep learning has made remarkable progress in generating realistic images (Goodfellow et al., 2014; Van Den Oord et al., 2017; Brock et al., 2019; Menick & Kalchbrenner, 2019; Ma et al., 2019; Razavi et al., 2019). Deep models usually learn the image distribution from the training data and then draw novel samples from it. Therefore, it is crucial that the training set correctly represents the distribution. However, in practice, the training set for the generative task can be corrupted and one needs to develop robust methods that aim to learn the uncorrupted distribution. In general, there are two types of corruption. The first one is when images themselves are defected or corrupted by noise. The second one is when the image dataset is corrupted by another category of images with different patterns, which are considered as outliers. In many real-world applications, corrupted datasets are inevitable during the data collection process and it is too expensive to clean up datasets. Even widely used datasets such as CIFAR-10 or ImageNet suffer from corruption and mislabeling (Northcutt et al., 2021). In addition, corruption may also occur when a new area of study is explored and it is unclear how to distinguish between normal and abnormal points. For example, in the beginning of the COVID-19 pandemic it was hard to diagnose COVID-19 patients and distinguish them from the rest of patients infected by a virus (Chowdhury et al., 2020; Xiao et al., 2020). In particular, the datasets of X-ray images of patients infected with COVID-19 may contain wrongly classified ones.

Figure 1. Demonstration of generation by VAE, VQ-VAE and RVQ-VAE with minor corruption: Given a training set of face images, where only 5% have masks, we trained VAE, VQ-VAE and RVQ-VAE models, and randomly generated ten examples from each model. VQ-VAE generated more outliers than normal faces, VAE generated only a few outliers but the images were blurry, and VQ-VAE generated normal faces without masks.

One may expect that a small portion of outliers in the training data should not affect the overall performance of a generative model. However, this is not true and even some state-of-the-art generative models may produce unexpected results when the training data is mildly corrupted. Indeed, the middle row of Fig. 1 demonstrates an image generation example with the common Vector Quantized-Variational Auto-Encoder (VQ-VAE) using a training set with 5%

[1]School of Mathematics, University of Minnesota, Twin Cities, USA [2]Division of Natural and Applied Sciences, Duke Kunshan University, Jiangsu, China. Correspondence to: Chieh-Hsin Lai <laixx313@umn.edu>, Dongmian Zou <dongmian.zou@dukekunshan.edu.cn>, Gilad Lerman <lerman@umn.edu>.

outliers, where VQ-VAE mainly learns from the outlier distribution of masked faces and generates more outliers than inliers. This intriguing observation strongly urges the development of robust generative methods, and in particular, robust VAE-type generating methods.

We are unaware of any work addressing the robustness of VAE-type generative models. Kaneko & Harada (2020) built robust generative adversarial networks (GANs) that could handle noisy images. Balaji et al. (2020) used a robust formulation of optimal transport in a Wasserstein GAN (Arjovsky et al., 2017) and demonstrated that they may handle a small fraction of outliers. However, both methods may not be sufficiently robust to outliers whose fractions are not too small.

In this work, we present an end-to-end model that makes the VQ-VAE framework robust to outliers in the training set. We call this model Robust VQ-VAE (RVQ-VAE). It uses two separate discrete latent spaces (codebooks) to encode the inliers and outliers. Iteratively, RVQ-VAE performs two main steps. The first one, which we refer to as *self-recognition*, assigns training data points to their corresponding codebooks according to the reconstruction errors. The second one, which we refer to as *joint-training*, updates the codebooks as well as the parameters of the encoder and the decoder by backpropagation. To some extent, this iterative process is similar to an EM algorithm (Dempster et al., 1977). However, both steps above are different from the ones of the EM algorithm and are novel in our context.

We remark that an additional novel subcomponent of the self-recognition step is "confidence"-based matching. It finds the best quantized vector in the codebook using a weighted Euclidean distance whose weights are determined according to the directional variances of the codebooks.

We experimentally validated our model using two different datasets, while corrupting their training points with different percentages of outliers. The consideration of many such percentages is rather time-consuming and extensive. Not only does our model successfully resolve the vulnerability of VQ-VAE to small corruption ratios, but it also proves to be robust to higher corruption ratios (up to 30%). In addition, our model is more robust to outliers than other robust generative models.

We briefly summarize the above contributions:

- RVQ-VAE is an end-to-end image generative VAE-type model, robust to outliers in the training data.
- It uses two separate codebooks to quantize inliers and outliers. Their iterative update has some novel components, such as the "confidence"-based matching.
- Numerical experiments indicate that RVQ-VAE outperforms other robust and non-robust models.

The rest of this paper is organized as follows. In §2 we review related previous works. In §3 we describe the details of the proposed method, RVQ-VAE. In §4 we test the robustness of RVQ-VAE while comparing it with competing methods. Lastly, we conclude this work in §5.

2. Related Works

Variational AutoEncoders (VAEs) (Kingma & Welling, 2019) and Generative Adversarial Networks (GANs)(Goodfellow et al., 2014) are well-studied generative models. VAEs have been applied to various generation tasks (Lotfollahi et al., 2020; Huang et al., 2018; Vahdat & Kautz, 2020). It is generally easier to train VAEs than GANs. However, GAN-based methods have been able to generate high-fidelity synthetic images (Arjovsky et al., 2017; Karras et al., 2020b;a; Zhao et al., 2020), whereas, until recently, VAE-based methods seemed to generate blurred images (Cai et al., 2019). In order to address this issue of low-quality generation, Van Den Oord et al. (2017) recently proposed the Vector Quantized-Variational AutoEncoder (VQ-VAE) framework. It uses a discrete latent space, or a codebook, containing a collection of vectors, where the number of vectors is a priori fixed and is much smaller than the dimension of the input data. The vectors (codes) in the codebook are updated throughout the training process. VQ-VAE uses this codebook to obtain a discrete, or "vectorized", latent representation of the output of the encoder by searching the nearest element in the codebook. We further review the VQ-VAE model in §3.1). Both VQ-VAE and its modified version, VQ-VAE-2 (Razavi et al., 2019), can generate high-fidelity images that are comparable to those generated by GAN-based methods (Brock et al., 2019). Although VQ-VAE was originally designed to handle both image and audio data, and was recently extended to other natural language processing tasks (van Niekerk et al., 2020), we only focus on its application to image generation.

Most VAE or GAN-based methods are not designed to handle corruption of the training set. Kaneko & Harada (2020) designed a family of GAN-based methods which can learn a clean generator from the training dataset corrupted by noise. Their method and its variations can be adapted to different noise models without complete prior information of the noise. Balaji et al. (2020) modified the Wasserstein distance in Wasserstein GAN (Arjovsky et al., 2017) by a robust formulation of optimal transport. They apply the method for image generation, where the training datasets are corrupted by only a small portion of outliers from other categories with distinct structures. Unlike these two methods, we aim to follow the VQ-VAE framework and consider relatively large fractions of outliers (up to 30%).

Reconstruction errors of autoencoders are widely used in detection of outliers in imaging data (Zhai et al., 2016; Zong et al., 2018; Perera et al., 2019; Zhou et al., 2021b;a; Li et al., 2021). To ensure that inliers have smaller errors and outliers

have larger ones, some previous works (Lai et al., 2020a;b) propose the use of sum of absolute deviations instead of squared distances for the loss function of the autoencoders. Our model also adopts such robust reconstruction error when determining which codebook each data point should be assigned to. In contrast to our model, in the above works the reconstruction error provides a score that is directly used for anomaly detection.

Weighted Euclidean distances are often adopted in detecting outliers. A common example is the Mahalanobis distance, which proves effective in both anomaly detection (Lee et al., 2018; Kamoi & Kobayashi, 2020; Hou et al., 2020) and generative networks (Mroueh & Sercu, 2017). Our distance is proportional to directional standard deviations (we later motivate this proportion), unlike the inverse proportion of the Mahalanobis distance.

3. Method

We review the VQ-VAE framework in §3.1 and describe our robust VQ-VAE-type method in §3.2.

3.1. The VQ-VAE framework for image generation

Unlike a regular VAE which encodes the input in a continuous latent space, VQ-VAE finds compressed representations of images by projecting the output of the encoder onto a discrete latent space. These representations aim to extract essential features of the images without distorting them too much, so the decoder may adequately reconstruct them. More precisely, the output of the encoder is quantized to a set of vectors, called the codebook , denoted by $\mathcal{C} := \left\{\boldsymbol{e}^{(i)}\right\}_{i=1}^{K} \subset \mathbb{R}^D$, where K is the size of the codebook and D is the dimension of the latent features. Given a data point $\boldsymbol{x}$ from the input dataset, let $\boldsymbol{z}_{\text{enc}}(\boldsymbol{x})$ denote the output of the encoder $\mathcal{E}$ of VQ-VAE, that is, $\boldsymbol{z}_{\text{enc}}(\boldsymbol{x}) := \mathcal{E}(\boldsymbol{x})$. The vectorized representation of $\boldsymbol{z}_{\text{enc}}(\boldsymbol{x})$, denoted by $\boldsymbol{z}_{\text{vq}}(\boldsymbol{x})$, is the nearest element in the codebook, that is,

$$\boldsymbol{z}_{\text{vq}}(\boldsymbol{x}) = \boldsymbol{e}^{(k)},\ k = \underset{1\le i\le K}{\arg\min} \left\|\boldsymbol{z}_{\text{enc}}(\boldsymbol{x}) - \boldsymbol{e}^{(i)}\right\|_2 . \quad (1)$$

This representation, $\mathbf{z}_{\text{vq}}(\boldsymbol{x})$, is then fed forward to the decoder $\mathcal{D}$. Given a training dataset $\mathcal{S}$, the parameters of the encoder and decoder, as well as the codebook, are updated by minimizing the following loss function:

$$\mathcal{L}_{\text{vqvae}}\left(\mathcal{E},\mathcal{C},\mathcal{D}\right) := \quad (2)$$
$$\mathbb{E}_{\boldsymbol{x}\sim\mathcal{S}}\Bigg\{\left\|\boldsymbol{x} - \mathcal{D}\Big(\boldsymbol{z}_{\text{enc}}(\boldsymbol{x}) + \text{sg}\left[\boldsymbol{z}_{\text{vq}}(\boldsymbol{x}) - \boldsymbol{z}_{\text{enc}}(\boldsymbol{x})\right]\Big)\right\|_2^2 +$$
$$\left\|\text{sg}\left[\boldsymbol{z}_{\text{enc}}(\boldsymbol{x})\right] - \boldsymbol{z}_{\text{vq}}(\boldsymbol{x})\right\|_2^2 + \beta\left\|\boldsymbol{z}_{\text{enc}}(\boldsymbol{x}) - \text{sg}\left[\boldsymbol{z}_{\text{vq}}(\boldsymbol{x})\right]\right\|_2^2\Bigg\},$$

where β is a hyperparameter and $\text{sg}[\cdot]$ is the stop-gradient operator (Bengio et al., 2013; Van Den Oord et al., 2017), which is the identity during the forward pass and has zero gradients during backward computation. The discrete latent indices, obtained by optimizing (2) are used for the training of the prior distribution of the VQ-VAE. This distribution is modeled by an autoregressive neural network, and its common choice is PixelCNN (Oord et al., 2016; Salimans et al., 2017) that follows the design of the VQ-VAE. Ultimately, the learned autoregressive prior is utilized for generation.

3.2. Description of RVQ-VAE

We assume that the training dataset is unlabeled and corrupted with outliers, whose fraction is at most 30%. For this setting, we propose RVQ-VAE, which follows the general framework of VQ-VAE. We first train an encoder and a decoder, together with a pair of codebooks, namely an inlier codebook and an outlier codebook. Then we learn a latent prior, which is modeled by PixelCNN, according to the codebooks. Finally, we use it for generation.

To train a good model that generates from the inlier distribution, we need to obtain a faithful inlier codebook. For this purpose, we iteratively apply two steps for training. The first one, which we refer to as *self-recognition*, classifies each data point as either an inlier or an outlier according to the reconstruction error from the previous stage. Each inlier or outlier is then quantized to a vector in the inlier or outlier codebook. Fig. 2 demonstrates the basic idea of self-recognition. The second step, which we refer to as *joint-training*, updates the parameters of all components of the autoencoder (the encoder, the decoder and the two codebooks) according to the quantization result. We further describe the two steps in detail below.

3.2.1. Self-recognition

We denote the inlier and outlier codebooks by $\mathcal{C}_{\text{in}} := \{\boldsymbol{e}_{\text{in}}^{(i)}\}_{i=1}^{K_{\text{in}}} \subset \mathbb{R}^D$ and $\mathcal{C}_{\text{out}} := \{\boldsymbol{e}_{\text{out}}^{(i)}\}_{i=1}^{K_{\text{out}}} \subset \mathbb{R}^D$, respectively, where K_{in} and K_{out} are the sizes of the inlier and outlier codebooks. We use more vectors in the inlier codebooks and therefore require that $K_{\text{in}} > K_{\text{out}}$.

The quantization process that maps $\boldsymbol{z}_{\text{enc}}$ to a code is similar to (1), but is different in two ways. First, we need to make a choice between $\mathcal{C}_{\text{in}}$ and $\mathcal{C}_{\text{out}}$. Second, we adopt a "confidence matching", in which the distance between $\boldsymbol{z}_{\text{enc}}$ and each code is weighted Euclidean. We clarify this quantization process as follows. Before training the VQ-VAE, we fix a hyperparameter η that bounds the percentage of data points associated with the outlier codebook. In general, $0 < \eta < 50\%$, though we fix the default parameter $\eta = 20\%$. In the first epoch, we have not received the reconstruction errors, and thus we temporarily treat all data points as inliers. For the consequent epochs, we re-label each data point as either an inlier or an outlier, according to its reconstruction error obtained from

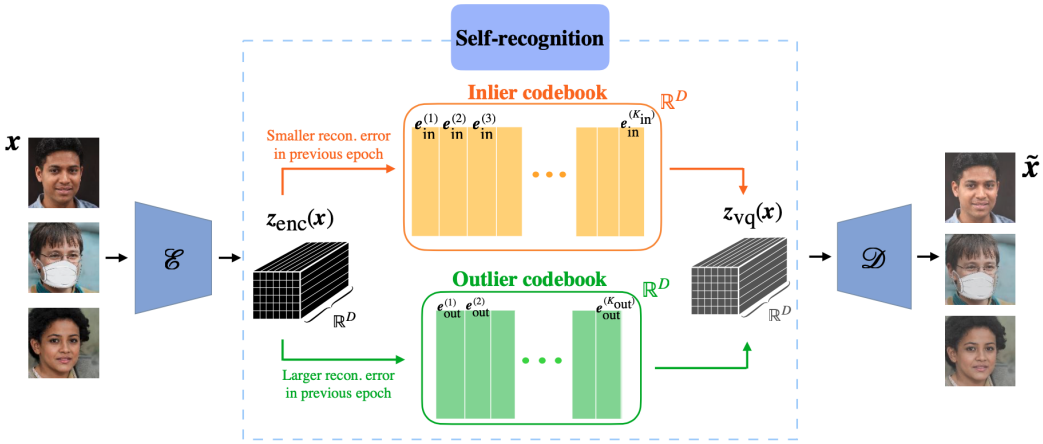

Figure 2. Illustration of the self-recognition step of RVQ-VAE. It uses two separate codebooks for inliers and outliers. The other step of joint-training updates $\mathcal{E}$ and $\mathcal{D}$ together with the codebooks.

the previous epoch. That is, we compute $\|\boldsymbol{x}-\tilde{\boldsymbol{x}}\|_2$ for each input data point $\boldsymbol{x}$ and its reconstructed point $\tilde{\boldsymbol{x}}=\mathcal{D}(\boldsymbol{z}_{\text{vq}}(\boldsymbol{x}))$ via the decoder from the previous epoch. The data points with top η (20% in our experiments) largest reconstruction errors are associated with the outlier codebook, while the rest with the inlier codebook. We next explain the assignment of inliers and outliers to vectors in their coodebooks, which we refer to as confidence matching and perform in each epoch.

For our proposed confidence matching, we replace the standard ℓ_2 distance in (1) with a weighted one, which introduces scaling in each direction. That is, for any two vectors $\boldsymbol{z}=(z_i)_{i=1}^D$ and $\boldsymbol{\mu}=(\mu_i)_{i=1}^D\in\mathbb{R}^D$ and a 'confidence" weight vector $\boldsymbol{s}=(s_i)_{i=1}^D\in\mathbb{R}^D$, the corresponding weighted Euclidean distance is

$$d_{\text{W}}(\boldsymbol{z};\boldsymbol{\mu},\boldsymbol{s}):=\sqrt{\sum_{i=1}^D s_i^2(z_i-\mu_i)^2}. \tag{3}$$

The coordinate s_i of $\boldsymbol{s}$ expresses the "confidence" in the i-th coordinate. In the confidence matching, for any input image $\boldsymbol{x}$ and any choice of inliers or outliers, we let $\boldsymbol{z}:=\boldsymbol{z}_{\text{enc}}(\boldsymbol{x})$ and $\boldsymbol{\mu}$ be the inlier or outlier codebook vectors. In this case we choose s_i as the standard deviation of the inlier or outlier codebook associated with $\boldsymbol{z}_{\text{enc}}(\boldsymbol{x})$ along the i-th coordinate. We find this choice for s_i as a natural "confidence score". Indeed, when we assign $\boldsymbol{z}_{\text{enc}}(\boldsymbol{x})$ to a vector, we are more confident about the directions where the set of possible vectors have a larger variance, so that they are far apart from each other. For a direction along which the variance of the vectors is small, we need to be more careful when we perform the quantization, because there is not much difference between the vectors and we do not lose much if we switch between them. Consequently, the quantization process may be unstable if we rely on such a direction. We remark that the loss function used for updating the codebooks employs the same distance (see the second and third terms in (7), which we will explain later). We experimentally noticed that when using the regular Euclidean distance instead, the norms of the codebook vectors dramatically increase and consequently the training process diverges. In principle, we could have used the full covariance of the codebook as the "confidence matrix". However, that would be computationally costly and significantly slow down the training process.

In summary, consider an input $\boldsymbol{x}$ from the training data. In the first epoch, we embed $\boldsymbol{z}_{\text{enc}}(\boldsymbol{x})$ to $\boldsymbol{z}_{\text{vq}}(\boldsymbol{x})$, the nearest point from the inlier codebook $\mathcal{C}_{\text{in}}$ using the weighted Euclidean distance. More precisely,

$$\boldsymbol{z}_{\text{vq}}(\boldsymbol{x})=\boldsymbol{e}_{\text{in}}^{(k)},\ k=\underset{1\le i\le K_{\text{in}}}{\arg\min}\, d_{\text{W}}(\boldsymbol{z}_{\text{enc}}(\boldsymbol{x});\boldsymbol{e}_{\text{in}}^{(i)},\text{std}(\mathcal{C}_{\text{in}})), \tag{4}$$

where $\text{std}(\mathcal{C}_{\text{in}})\in\mathbb{R}^D$ is the vector composed of the standard deviations of the inlier codebook $\mathcal{C}_{\text{in}}$ in all coordinates:

$$\text{std}(\mathcal{C}_{\text{in}})_j=\text{std}\left(\left\{\boldsymbol{e}_{\text{in},j}^{(i)}\right\}_{i=1}^{K_{\text{in}}}\right),\quad j=1,\cdots,D, \tag{5}$$

where $\boldsymbol{e}_{\text{in},j}^{(i)}$ is the j-th entry of $\boldsymbol{e}_{\text{in}}^{(i)}$. For all the consequent epochs, if $\|\boldsymbol{x}-\tilde{\boldsymbol{x}}\|_2$, the reconstruction error for $\boldsymbol{x}$, is not among the largest η of all errors, we update $\boldsymbol{z}_{\text{vq}}$ according to (4) again. Otherwise, we search $\boldsymbol{z}_{\text{vq}}(\boldsymbol{x})$ from the outlier codebook $\mathcal{C}_{\text{out}}$:

$$\boldsymbol{z}_{\text{vq}}(\boldsymbol{x})=\boldsymbol{e}_{\text{out}}^{(k)},\ k=\underset{1\le i\le K_{\text{out}}}{\arg\min}\, d_{\text{W}}(\boldsymbol{z}_{\text{enc}}(\boldsymbol{x});\boldsymbol{e}_{\text{out}}^{(i)},\text{std}(\mathcal{C}_{\text{out}})), \tag{6}$$

where $\text{std}(\mathcal{C}_{\text{out}})$ is the vector of standard deviations for the outlier codebook $\mathcal{C}_{\text{out}}$, which is defined similarly to (5).

3.2.2. Joint-training

In each epoch, after associating with the training data specific vectors in the codebooks, we propose using the following

robust loss function for updating the parameters of the encoder $\mathcal{E}$, decoder $\mathcal{D}$ and the two codebooks $\mathcal{C}_{\text{in}}$ and $\mathcal{C}_{\text{out}}$:

$$\begin{aligned}
&\mathcal{L}_{\text{rvqvae}}\left(\mathcal{E}, \mathcal{C}_{\text{in}}, \mathcal{C}_{\text{out}}, \mathcal{D}\right) \\
:=&\mathbb{E}_{\boldsymbol{x}\sim\mathcal{S}}\Bigg\{\left\|\boldsymbol{x}-\mathcal{D}\Big(\boldsymbol{z}_{\text{enc}}(\boldsymbol{x})+\text{sg}\left[\boldsymbol{z}_{\text{vq}}(\boldsymbol{x})-\boldsymbol{z}_{\text{enc}}(\boldsymbol{x})\right]\Big)\right\|_2 \\
&+d_M\Big(\text{sg}\left[\boldsymbol{z}_{\text{enc}}(\boldsymbol{x})\right];\boldsymbol{z}_{\text{vq}}(\boldsymbol{x}),\text{std}(\mathcal{C}(\boldsymbol{x}))\Big) \qquad (7)\\
&+\beta d_M\Big(\text{sg}\left[\boldsymbol{z}_{\text{vq}}(\boldsymbol{x})\right];\boldsymbol{z}_{\text{enc}}(\boldsymbol{x}),\text{std}(\mathcal{C}(\boldsymbol{x}))\Big)\Bigg\},
\end{aligned}$$

where $\text{std}(\mathcal{C}(\boldsymbol{x}))=\mathcal{C}_{\text{in}}$ if $\boldsymbol{x}$ is associated with the inlier codebook and $\text{std}(\mathcal{C}(\boldsymbol{x}))=\mathcal{C}_{\text{out}}$ otherwise. To ensure robustness in the early stage of training, when the assignment of the codebook might be wrong, we use least-absolute-deviations minimization (which avoids squaring each term in (7)), and was advocated in Lerman & Maunu (2018); Lai et al. (2020b;a). We emphasize that we use the weighted Euclidean distance of (3) (see second and third terms of (7)), which was already used for quantization in (4) and (6).

Once the RVQ-VAE is trained, we only utilize the inlier codebook to obtain the discrete latent indices $\{k^{(t)}\}_{t=1}^{L} \subset \{1,2,\cdots,K_{\text{in}}\}$ of the training dataset $\{\boldsymbol{x}^{(t)}\}_{t=1}^{L}$. Namely, for each $\boldsymbol{x}^{(t)}$ where $t=1,\cdots,L$, we search for the index $k^{(t)}$ by computing

$$k^{(t)}=\underset{1\le i\le K_{\text{in}}}{\arg\min}\, d_{\text{W}}(\boldsymbol{z}_{\text{enc}}(\boldsymbol{x}^{(t)});\boldsymbol{e}_{\text{in}}^{(i)},\text{std}(\mathcal{C}_{\text{in}})). \qquad (8)$$

The training of RVQ-VAE is summarized as Algorithm 1 in Appendix A. The discrete latent indices are further used for training the PixelCNN and then the sampling procedure is identical as that of a regular VQ-VAE (Van Den Oord et al., 2017).

4. Experiments

4.1. Baselines

We compare RVQ-VAE with the following methods for image generation: VQ-VAE (Van Den Oord et al., 2017), GAN (Goodfellow et al., 2014), Noise Robust GAN (NR-GAN) (Kaneko & Harada, 2020) and Robust Optimal Transport (Robust OT) (Balaji et al., 2020). While the details of VQ-VAE were presented in §3.1, we describe the other methods as follows.

GAN learns the data distribution via adversarial training. It contains two components of neural networks: a generator and a discriminator. The generator learns to map a simple noise to the data distribution. On the other hand, the discriminator learns to distinguish candidates produced by the generator from the true data distribution.

NR-GAN is a GAN-based method that aims to learn a clean image generator while the training set is noisy. It trains a clean image generator and noise generator simultaneously with a distribution or transformation constraint on the noise generator. We choose one of the variants of NR-GAN, namely SD-NR-GAN-III, which does not assume a specific prior noise and better aligns with our task.

Robust OT designs a robust formulation of Wasserstein distance according to a constrained form of duality. Their distance is insensitive to outliers and can prevent the corresponding Wasserstein GAN from learning from outliers. To the best of our knowledge, this work is the only one in the literature that intentionally addresses the robust generation problem without assuming a specific noise form.

We implement the VQ-VAE model by modifying the code in https://github.com/deepmind/sonnet/blob/v2/examples/vqvae_example.ipynb to a PyTorch version. We implement both GAN and NR-GAN using the official code provided in Kaneko & Harada (2020), and implemented Robust OT using the official code provided in Balaji et al. (2020). We will make all codes available once we get an approval from the patent office handling a related invention.

4.2. Datasets and settings

Figure 3. Sample images from FaceMask and RoomCrop.

We report results on two image datasets: FaceMask and RoomCrop. Each dataset contains an inlier class and an outlier class. We demonstrate random examples from them in Fig 3. We consider the following outlier ratios (fraction of outliers from all data points): 0%, 5%, 10%, 15%, 20%, 25%, 30%. For each dataset, ratio and baseline model, we train a generative model.

FaceMask contains 64×64 human face images downsized from the 1024×1024 images in Kottarathil (2020). There are two classes: unmasked faces and masked faces with 10,000 images in each. For each experiment, we take all 10,000 unmasked faces as inliers and randomly choose outliers to have a chosen ratio.

RoomCrop is constructed from the LSUN dataset(Yu et al., 2015) in the following way. We randomly sample 60,000 images from the "bedroom" category of LSUN and downsize them to 64×64. After that, we split the images into two subsets, each containing 30,000 images. The first subset is kept as inliers. For each image in the second subset of outliers, we randomly choose the number of cropped rectangles to be 1, 2 or 3. For each rectangle we randomly choose a center and area between 15 and 25 and replace

its pixel values to be black. The second subset is used as outliers. For each experiment, we take all 30,000 inliers and randomly choose outliers to have a chosen ratio.

The encoder of RVQ-VAE is composed of 3 convolutional layers with kernel size $(4, 4, 3)$, output channels $(64, 128, 128)$ and stride $(2, 2, 1)$, followed by 2 residual blocks, consisting of a convolutional layer with kernel size 3 and a convolutional layer with kernel size 1. The decoder of RVQ-VAE has a deconvolutional layer with kernel size 3, output channel 128, stride 1, followed by two residual blocks and 2 deconvolutional layers with kernel size $(4, 4)$, output channels $(64, 3)$, and stride $(2, 2)$, respectively. In the neural network, the activation functions are all taken to be ReLU. The dimension of the two codebook vectors are $D = 64$. The size of the inlier codebook is $K_{\text{in}} = 512$ and of the outlier codebook is $K_{\text{out}} = 256$. The threshold is $\eta = 20\%$ and the regularization weight is $\beta = 0.25$. The neural networks are optimized by Adam (Kingma & Ba, 2015) with a learning rate $3e-4$ and trained for 400 epochs with a batch size of 10.

4.3. Metrics and results

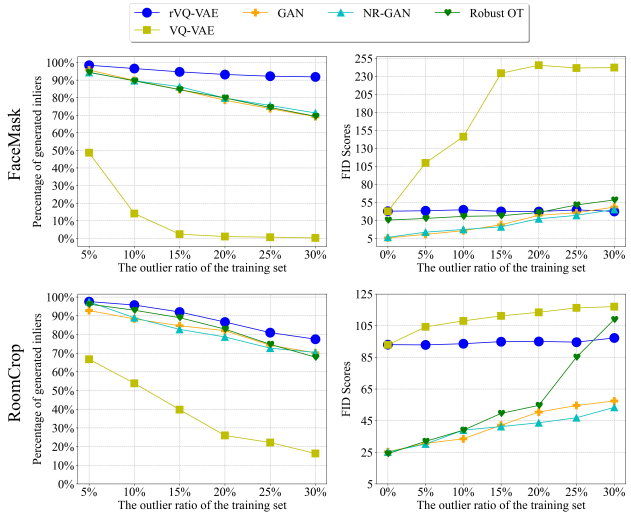

Figure 4. Percentage of generated inliers (on left) and FID scores (on right) for the baseline methods using the FaceMask and RoomCrop datasets. The inliers are recognized by a well-trained classifier.

To evaluate the percentage of outliers in the generated examples, we train a binary classifier with the following neural network structure: 2 convolutional layers with kernel size $(3, 3)$, output channel $(32, 64)$, stride $(2, 2)$, and ReLU activation functions. The convolutional layers are followed by a max pooling layer and 2 dropout layers with ratio $(0.25, 0.5)$. These are followed by a flatten layer and fully connected layers with output channel $(3136, 128, 2)$. At last, we apply the softmax function to produce the probability of each class. The classifier is trained using the same number of inliers and outliers.

For each dataset and model, we generate the same number of examples as the number of inliers in the training set. Then we apply the binary classifier to determine the percentage of inliers within the generated images. To quantitatively measure the quality of images generated by each method, we also compute the Fréchet Inception Distance (FID) (Karras et al., 2020b) between the set of generated images and the images of the inlier class. Fig. 4 reports both the percentage of generated inliers and FID scores for all methods and outlier ratios.

To visualize the generated images, we further plot 100 samples generated by each method with outlier ratios 5%, 15%, 25%, 30% for FaceMask and RoomCrop in Figs 5 and 6, respectively. We present the generated images with outlier ratios 0%, 10% and 20% in the supplemental material.

In terms of the percentage of generated inliers, we note that VQ-VAE almost only generates abnormal images when the outlier ratios of the training set for FaceMask are greater than 10%. Its performance is also poor for RoomCrop. As the outlier ratio increases, the GAN-based methods, including GAN, NR-GAN and the robust OT, do not seem to be robust at all, because the proportion of outliers generated is similar to the outlier ratio in the training set. In contrast, RVQ-VAE produces significantly less outliers in the generated examples.

In terms of FID, GAN-based models have lower FID scores than VQ-VAE or RVQ-VAE, that is, their quality is better. Note that when there are no outliers in the training data, VQ-VAE also produces a relatively larger FID (see supplementary material for visualization). This suggests that the large FID of RVQ-VAE is not due to our regime, but due to the fact that the VQ-VAE cannot produce images of the same quality as GAN in this generative task. We also note that images generated by either RVQ-VAE or VQ-VAE have similar quantities. That is, RVQ-VAE does not sacrifice the quality of VQ-VAE for robustness. Lastly, we observe that for the GAN-based models, the FID increases when the outlier ratio in the training set increases. In contrast, for RVQ-VAE, the FID stays almost constant, implying that the fraction of outliers in the generated examples did not significantly increase.

5. Conclusion and future works

We present RVQ-VAE, a novel robust generative model within the framework of VQ-VAE. Our central idea is to iteratively update two codebooks for inliers and outliers and only employ the inlier codebook for generation. By confidence-matching we rescale the importance of the coordinates and consequently improve the stability in the quantization process. Our model is more robust to outliers in the training set, compared with the other robust generative models.

We noted in §4.3 that VQ-VAE and thus also RVQ-VAE do

Figure 5. 100 synthetic images of FaceMask generated by RVQ-VAE and competing methods. From the left to right columns are the results obtained by training on the dataset with outlier ratios $= 5\%, 15\%, 25\%$ and 30%, respectively.

not generate images of the same quality as GANs. Nevertheless, robust GAN-based models are not robust for the tasks we considered, especially when the percentage of outliers is nontrivial. In order to improve the quality of the generated images, we will try to extend our work to more advanced frameworks such as VQ-VAE-2. We also plan to extend our ideas to other VAE structures that have a discrete latent space.

We do not consider the case where the inliers may belong to multiple classes, where it will be more difficult to distinguish between inliers and outliers. In future work we may consider multiple codebooks for the inliers to address this scenario.

Figure 6. 100 synthetic images of RoomCrop generated by RVQ-VAE and competing methods. From the left to right columns are the results obtained by training on the dataset with outlier ratios $= 5\%, 15\%$, 25% and 30%, respectively.

We considered specific datasets with corrupted images. We noticed that current GAN-based robust models were not sufficiently robust to the outliers in these datasets. In the future, we would like to study more extensively different types of datasets and carefully characterize successes and failures of RVQ-VAE and other algorithms. We would also like to extend this study to audio and video data.

Lastly, we expect we can extend the presented model to address the different problem of anomaly detection.

References

Arjovsky, M., Chintala, S., and Bottou, L. Wasserstein generative adversarial networks. In *International conference on machine learning*, pp. 214–223. PMLR, 2017.

Balaji, Y., Chellappa, R., and Feizi, S. Robust optimal transport with applications in generative modeling and domain adaptation. In *Advances in Neural Information Processing Systems*, volume 33, pp. 12934–12944, 2020. URL https://proceedings.neurips.cc/paper/2020/file/9719a00ed0c5709d80dfef33795dcef3-Paper.pdf.

Bengio, Y., Léonard, N., and Courville, A. Estimating or propagating gradients through stochastic neurons for conditional computation. *arXiv preprint arXiv:1308.3432*, 2013.

Brock, A., Donahue, J., and Simonyan, K. Large scale GAN training for high fidelity natural image synthesis. In *International Conference on Learning Representations*, 2019. URL https://openreview.net/forum?id=B1xsqj09Fm.

Cai, L., Gao, H., and Ji, S. Multi-stage variational auto-encoders for coarse-to-fine image generation. In *Proceedings of the 2019 SIAM International Conference on Data Mining*, pp. 630–638. SIAM, 2019.

Chowdhury, M. E., Rahman, T., Khandakar, A., Mazhar, R., Kadir, M. A., Mahbub, Z. B., Islam, K. R., Khan, M. S., Iqbal, A., Al Emadi, N., et al. Can AI help in screening viral and covid-19 pneumonia? *IEEE Access*, 8:132665–132676, 2020.

Dempster, A. P., Laird, N. M., and Rubin, D. B. Maximum likelihood from incomplete data via the EM algorithm. *Journal of the Royal Statistical Society: Series B (Methodological)*, 39 (1):1–22, 1977.

Goodfellow, I., Pouget-Abadie, J., Mirza, M., Xu, B., Warde-Farley, D., Ozair, S., Courville, A., and Bengio, Y. Generative adversarial nets. In *Advances in Neural Information Processing Systems*, pp. 2672–2680, 2014.

Hou, Y., Chen, Z., Wu, M., Foo, C.-S., Li, X., and Shubair, R. M. Mahalanobis distance based adversarial network for anomaly detection. In *ICASSP 2020-2020 IEEE International Conference on Acoustics, Speech and Signal Processing (ICASSP)*, pp. 3192–3196. IEEE, 2020.

Huang, H., He, R., Sun, Z., Tan, T., et al. IntroVAE: Introspective variational autoencoders for photographic image synthesis. *Advances in Neural Information Processing Systems*, 31, 2018.

Kamoi, R. and Kobayashi, K. Why is the Mahalanobis distance effective for anomaly detection? *arXiv preprint arXiv:2003.00402*, 2020.

Kaneko, T. and Harada, T. Noise robust generative adversarial networks. In *Proceedings of the IEEE/CVF Conference on Computer Vision and Pattern Recognition*, pp. 8404–8414, 2020.

Karras, T., Aittala, M., Hellsten, J., Laine, S., Lehtinen, J., and Aila, T. Training generative adversarial networks with limited data. *arXiv preprint arXiv:2006.06676*, 2020a.

Karras, T., Laine, S., Aittala, M., Hellsten, J., Lehtinen, J., and Aila, T. Analyzing and improving the image quality of StyleGAN. In *Proceedings of the IEEE/CVF Conference on Computer Vision and Pattern Recognition*, pp. 8110–8119, 2020b.

Kingma, D. P. and Ba, J. Adam: A method for stochastic optimization. In *International Conference on Learning Representations*, 2015.

Kingma, D. P. and Welling, M. An introduction to variational autoencoders. *Foundations and Trends® in Machine Learning*, 12 (4):307–392, 2019. ISSN 1935-8237. doi: 10.1561/2200000056. URL http://dx.doi.org/10.1561/2200000056.

Kottarathil, P. Face mask lite dataset https://www.kaggle.com/prasoonkottarathil/face-mask-lite-dataset, 2020.

Lai, C.-H., Zou, D., and Lerman, G. Novelty detection via robust variational autoencoding, 2020a. arXiv preprint arXiv:2006.05534.

Lai, C.-H., Zou, D., and Lerman, G. Robust subspace recovery layer for unsupervised anomaly detection. In *International Conference on Learning Representations*, 2020b. URL https://openreview.net/forum?id=rylb3eBtwr.

Lee, K., Lee, K., Lee, H., and Shin, J. A simple unified framework for detecting out-of-distribution samples and adversarial attacks. *Advances in neural information processing systems*, 31, 2018.

Lerman, G. and Maunu, T. An overview of robust subspace recovery. *Proceedings of the IEEE*, 106(8):1380–1410, 2018. doi: 10.1109/JPROC.2018.2853141.

Li, T., Wang, Z., Liu, S., and Lin, W.-Y. Deep unsupervised anomaly detection. In *Proceedings of the IEEE/CVF Winter Conference on Applications of Computer Vision*, pp. 3636–3645, 2021.

Lotfollahi, M., Naghipourfar, M., Theis, F. J., and Wolf, F. A. Conditional out-of-distribution generation for unpaired data using transfer VAE. *Bioinformatics*, 36(Supplement_2):i610–i617, 2020.

Ma, X., Kong, X., Zhang, S., and Hovy, E. Macow: Masked convolutional generative flow. *Advances in Neural Information Processing Systems*, 32:5893–5902, 2019.

Menick, J. and Kalchbrenner, N. Generating high fidelity images with subscale pixel networks and multidimensional upscaling. In *International Conference on Learning Representations*, 2019. URL https://openreview.net/forum?id=HylzTiC5Km.

Mroueh, Y. and Sercu, T. Fisher GAN. In *Proceedings of the 31st International Conference on Neural Information Processing Systems*, pp. 2510–2520, 2017.

Northcutt, C. G., Athalye, A., and Mueller, J. Pervasive label errors in test sets destabilize machine learning benchmarks. In *Thirty-fifth Conference on Neural Information Processing Systems Datasets and Benchmarks Track (Round 1)*, 2021. URL https://openreview.net/forum?id=XccDXrDNLek.

Oord, A. v. d., Kalchbrenner, N., Vinyals, O., Espeholt, L., Graves, A., and Kavukcuoglu, K. Conditional image generation with pixelcnn decoders. *arXiv preprint arXiv:1606.05328*, 2016.

Perera, P., Nallapati, R., and Xiang, B. OCGAN: One-class novelty detection using gans with constrained latent representations. In *Proceedings of the IEEE Conference on Computer Vision and Pattern Recognition*, pp. 2898–2906, 2019.

Razavi, A., van den Oord, A., and Vinyals, O. Generating diverse high-fidelity images with VQ-VAE-2. In *Advances in Neural Information Processing Systems*, pp. 14866–14876, 2019.

Salimans, T., Karpathy, A., Chen, X., and Kingma, D. P. PixelCNN++: Improving the PixelCNN with discretized logistic mixture likelihood and other modifications. In *International Conference on Learning Representations*, 2017.

Vahdat, A. and Kautz, J. NVAE: A deep hierarchical variational autoencoder. In *Advances in Neural Information Processing Systems*, volume 33, pp. 19667–19679, 2020. URL https://proceedings.neurips.cc/paper/2020/file/e3b21256183cf7c2c7a66be163579d37-Paper.pdf.

Van Den Oord, A., Vinyals, O., et al. Neural discrete representation learning. In *Advances in Neural Information Processing Systems*, pp. 6306–6315, 2017.

van Niekerk, B., Nortje, L., and Kamper, H. Vector-quantized neural networks for acoustic unit discovery in the zerospeech 2020 challenge. *arXiv preprint arXiv:2005.09409*, 2020.

Xiao, A. T., Tong, Y. X., and Zhang, S. False-negative of RT-PCR and prolonged nucleic acid conversion in COVID-19: Rather than recurrence. *Journal of Medical Virology*, 2020.

Yu, F., Seff, A., Zhang, Y., Song, S., Funkhouser, T., and Xiao, J. LSUN: Construction of a large-scale image dataset using deep learning with humans in the loop. *arXiv preprint arXiv:1506.03365*, 2015.

Zhai, S., Cheng, Y., Lu, W., and Zhang, Z. Deep structured energy based models for anomaly detection. In *Proceedings of The 33rd International Conference on Machine Learning*, volume 48, pp. 1100–1109. PMLR, 2016.

Zhao, Y., Li, C., Yu, P., Gao, J., and Chen, C. Feature quantization improves GAN training. In *Proceedings of the 37th International Conference on Machine Learning*, volume 119, pp. 11376–11386. PMLR, 2020.

Zhou, K., Li, J., Luo, W., Li, Z., Yang, J., Fu, H., Cheng, J., Liu, J., and Gao, S. Proxy-bridged image reconstruction network for anomaly detection in medical images. *IEEE Transactions on Medical Imaging*, 2021a.

Zhou, K., Li, J., Xiao, Y., Yang, J., Cheng, J., Liu, W., Luo, W., Liu, J., and Gao, S. Memorizing structure-texture correspondence for image anomaly detection. *IEEE Transactions on Neural Networks and Learning Systems*, 2021b.

Zong, B., Song, Q., Min, M. R., Cheng, W., Lumezanu, C., Cho, D., and Chen, H. Deep autoencoding gaussian mixture model for unsupervised anomaly detection. In *International Conference on Learning Representations*, 2018.

A. Algorithm of RVQ-VAE

Algorithm 1 Training RVQ-VAE

Input: Training dataset $\{\boldsymbol{x}^{(t)}\}_{t=1}^{L}$; initialized parameters of $\mathcal{E}$ and $\mathcal{D}$; initialized codebooks: $\mathcal{C}_{\text{in}} = \{\boldsymbol{e}_{\text{in}}^{(i)}\}_{i=1}^{K_{\text{in}}}$ and $\mathcal{C}_{\text{out}} = \{\boldsymbol{e}_{\text{out}}^{(i)}\}_{i=1}^{K_{\text{out}}} \subset \mathbb{R}^D$; threshold η; regularization weight β; number of epochs T; batch size I; learning rate α
Output: Trained parameters of $\mathcal{E}$ and $\mathcal{D}$; trained inlier codebook $\mathcal{C}_{\text{in}}$; discrete latent indices $\{k^{(t)}\}_{t=1}^{L}$ of $\{\boldsymbol{x}^{(t)}\}_{t=1}^{L}$

for epoch $\tau = 1, \cdots, T$ **do**
  for each batch $\{\boldsymbol{x}^{(t)}\}_{t\in\mathcal{I}}$ **do**
    if $\tau = 1$ **then**
      $k^{(t)} \leftarrow \underset{1\le i\le K_{\text{in}}}{\arg\min}\, d_{\text{W}}(\boldsymbol{z}_{\text{enc}}(\boldsymbol{x}^{(t)}); \boldsymbol{e}_{\text{in}}^{(i)}, \text{std}(\mathcal{C}_{\text{in}}))$
      $\boldsymbol{z}_{\text{vq}}(\boldsymbol{x}^{(t)}) \leftarrow \boldsymbol{e}_{\text{in}}^{k^{(t)}}$
    else
      $\mathcal{I}_{\text{out}} \leftarrow$ indices of the top $\lceil \eta \times |\mathcal{I}| \rceil\}$ elements of $\{\text{Err}(\tau-1)^{(t)}\}_{t\in\mathcal{I}}$
      if $t \in \mathcal{I}_{\text{out}}$ **then**
        $k^{(t)} \leftarrow \underset{1\le i\le K_{\text{out}}}{\arg\min} d_{\text{W}}(\boldsymbol{z}_{\text{enc}}(\boldsymbol{x}^{(t)}); \boldsymbol{e}_{\text{out}}^{(i)}, \text{std}(\mathcal{C}_{\text{out}}))$
        $\boldsymbol{z}_{\text{vq}}(\boldsymbol{x}^{(t)}) \leftarrow \boldsymbol{e}_{\text{out}}^{k^{(t)}}$
      else
        $k^{(t)} \leftarrow \underset{1\le i\le K_{\text{in}}}{\arg\min}\, d_{\text{W}}(\boldsymbol{z}_{\text{enc}}(\boldsymbol{x}^{(t)}); \boldsymbol{e}_{\text{in}}^{(i)}, \text{std}(\mathcal{C}_{\text{in}}))$
        $\boldsymbol{z}_{\text{vq}}(\boldsymbol{x}^{(t)}) \leftarrow \boldsymbol{e}_{\text{in}}^{k^{(t)}}$
      end if
    end if
    $\tilde{\boldsymbol{x}}^{(t)} \leftarrow \mathcal{D}(\boldsymbol{z}_{\text{vq}}(\boldsymbol{x}^{(t)}))$
    $\text{Err}(\tau)^{(t)} \leftarrow \left\|\boldsymbol{x}^{(t)} - \tilde{\boldsymbol{x}}^{(t)}\right\|_2$
    $(\mathcal{E}, \mathcal{C}_{\text{in}}, \mathcal{C}_{\text{out}}, \mathcal{D}) \leftarrow (\mathcal{E}, \mathcal{C}_{\text{in}}, \mathcal{C}_{\text{out}}, \mathcal{D})$
      $-\alpha\nabla_{(\mathcal{E},\mathcal{C}_{\text{in}},\mathcal{C}_{\text{out}},\mathcal{D})}\mathcal{L}_{\text{rvqvae}}(\mathcal{E}, \mathcal{C}_{\text{in}}, \mathcal{C}_{\text{out}}, \mathcal{D})$
    according to (7)
  end for
end for
Obtain the trained $\mathcal{E}$ and $\mathcal{C}_{\text{in}}$
for each $t = 1, \cdots, L$ **do**
  $k^{(t)} \leftarrow \underset{1\le i\le K_{\text{in}}}{\arg\min}\, d_{\text{W}}(\boldsymbol{z}_{\text{enc}}(\boldsymbol{x}^{(t)}); \boldsymbol{e}_{\text{in}}^{(i)}, \text{std}(\mathcal{C}_{\text{in}}))$
end for

B. Additional generated images

Figs. 7 and 8 extend the demonstration in Figs. 5 and 6 of the main text, by considering the following outlier ratios: 0%, 10% and 20% (recall that the earlier figures considered 5%, 15% and 25%). These figures were not shown in the main text due to page limit.

For each method (RVQ-VAE, VQ-VAE, robust OT, GAN and NR-GAN) and outlier ratio, Figs. 7 and 8 demonstrate 100 generated images for FaceMask and RoomCrop , respectively.

C. Numerical representations for some figures

We present the numerical values depicted in Fig. 4 of the main text as tables.

D. Effectiveness of the binary classifier

In order to illustrate the effectiveness of the classifier used to evaluate the percentage of outliers in the generated examples, we report the F1 scores on labeled test data. Table 5 records the F1 scores of the trained classifier for the following outlier

Table 1. Percentage of generated inliers for FaceMask

	Training outlier ratios					
Methods	5%	10%	15%	20%	25%	30%
RVQ-VAE	**98.42%**	**96.55%**	**94.67%**	**93.18%**	**92.18%**	**91.81%**
VQ-VAE	48.68%	14.08%	2.34%	0.98%	0.62%	0.22%
robust OT	94.44%	89.55%	84.53%	79.80%	74.41%	69.39%
GAN	95.73%	89.83%	84.60%	78.51%	73.75%	69.11%
NR-GAN	94.29%	89.64%	86.24%	79.78%	75.52%	71.29%

Table 2. Percentage of generated inliers for RoomCrop

	Training outlier ratios					
Methods	5%	10%	15%	20%	25%	30%
RVQ-VAE	**97.56%**	**95.72%**	**91.98%**	**86.64%**	**80.96%**	**77.44%**
VQ-VAE	66.71%	53.85%	39.75%	25.93%	22.15%	16.29%
robust OT	96.19%	92.94%	88.95%	82.85%	72.71%	67.80%
GAN	92.78%	88.91%	84.63%	82.00%	74.23%	70.15%
NR-GAN	97.43%	88.91%	82.69%	78.65%	72.64%	70.36%

Table 3. FID scores of generated images for FaceMask

	Training outlier ratios						
Methods	0%	5%	10%	15%	20%	25%	30%
RVQ-VAE	42.723	43.367	44.680	42.496	42.340	44.552	**42.537**
VQ-VAE	42.659	100.767	146.244	234.322	245.413	241.596	242.206
robust OT	30.420	32.670	35.593	36.400	40.971	51.398	58.344
GAN	**5.681**	**10.578**	**15.675**	**23.871**	**37.029**	**40.558**	48.488
NR-GAN	6.381	13.650	17.358	21.060	32.201	36.971	45.143

Table 4. FID scores of generated images for RoomCrop

	Training outlier ratios						
Methods	0%	5%	10%	15%	20%	25%	30%
RVQ-VAE	92.987	92.831	93.574	94.891	95.026	94.578	97.213
VQ-VAE	92.816	104.214	107.996	111.145	113.437	116.230	117.203
robust OT	24.062	31.880	38.935	49.554	54.691	85.075	108.884
GAN	**23.301**	30.595	**33.507**	42.098	50.377	54.553	57.381
NR-GAN	25.137	**30.184**	38.976	**41.260**	**43.630**	**46.796**	**53.351**

ratios of the testing set: 0%, 5%, 10%, 15%, 20%, 25%, 30%. Since the classifier we employed showed almost perfect F1 scores, the large margin of our model over other ones is validated

Table 5. Testing F1 scores of the trained binary classifier on FaceMask and RoomCrop

	Testing outlier ratios						
Datasets	0%	5%	10%	15%	20%	25%	30%
FaceMask	1.000	1.000	1.000	0.995	0.996	0.984	0.979
RoomCrop	0.997	0.989	0.968	0.970	0.966	0.959	0.934

Figure 7. 100 synthetic images of FaceMask generated by RVQ-VAE and competing methods for outlier ratios 0%, 10% and 20% (from left to right).

Figure 8. 100 synthetic images of RoomCrop generated by RVQ-VAE and competing methods for outlier ratios 0%, 10% and 20% (from left to right).